# Ultrathin Resistive Sheets for Broadband Coherent Absorption and Symmetrization of Acoustic Waves

M. Farooqui,* Y. Aurégan,† and V. Pagneux‡
*Laboratoire d'Acoustique de l'Université du Mans (LAUM), UMR 6613 CNRS, Le Mans Université, Avenue O. Messiaen, Le Mans cedex 9 72085, France*

(Received 8 December 2021; revised 23 March 2022; accepted 12 May 2022; published 5 July 2022)

The manipulation of acoustic waves is experimentally and theoretically investigated based on the concept of coherent perfect absorption. It is shown that the absolute control of antisymmetric modes of an acoustic duct is possible using an ultrathin wire mesh. By varying the relative phase of two counterpropagating (normal or oblique) incident waves, the absorption due to wire mesh can be tuned from zero to unity. Experimental as well as numerical results demonstrate that this phenomenon is extremely broadband—allowing, for instance, the symmetrization of the acoustic wave with a short pulse in the time domain.

DOI: 10.1103/PhysRevApplied.18.014007

## I. INTRODUCTION

The search for new ways to absorb waves is still very active and, more particularly, in acoustics due to the continuous demand in noise control for a quiet environment. The most classical sound absorbers are made of porous parts that allow broadband attenuation at high frequencies but that remain low-pass filters and thus are inefficient at low frequencies. In the past decade, many types of metamaterial absorbers [1–4] have been proposed. They all are based on the use of subwavelength resonances, with finely tuned parameters that provide up to perfect absorption near the resonance frequencies, and they are inherently inefficient in the limit of zero frequency. One step further has been achieved recently by the introduction of the concept of the coherent perfect absorber (CPA), to control and to tune the rate of absorption [5–10]. It corresponds to the time reversal of a laser [5,6,11] and it uses the tuning of the incident waves from each side of the absorber.

It appears that a challenging task remains: to absorb sound near the zero-frequency limit while remaining broadband. Indeed, when using typical subwavelength resonators, the quality factor of the absorption peak of the resonance frequency increases when this frequency goes to zero [12,13]. The avoidance of resonance is a solution to obtain broadband low-frequency absorption, as demonstrated by metallic conductive films [14,15], where CPA with total absorption is possible. In the domain of airborne acoustics, ultrathin millimetric resistive sheets offer the same possibilities [16,17]. Often called wire mesh, their efficiency has no lower-bound limit on the frequency; they are used even for static flow—for instance, in filtration—and they remain efficient up to high frequencies as long as the wavelength is larger than the millimetric thickness.

In this paper, we present experimental and numerical evidence of the low- and midfrequency-absorption possibilities of ultrathin resistive sheets. After showing the capabilities of CPA for scattering, we apply it in a symmetric closed cavity, where it has important and natural impacts: when the absorber is at the center of symmetry of the cavity, the antisymmetric waves are totally absorbed. Since the resistive sheets are very thin compared to typical audible airborne acoustic wavelengths, the cancellation of the antisymmetric acoustic field is very broadband and it allows us to demonstrate it experimentally in the time domain with short pulses. We also take advantage of the wide bandwidth of this effect to design cavities where the sound field is symmetrized independently of the source position over a broad frequency range.

## II. BROADBAND COHERENT ABSORPTION

Let us begin with a description of the system at hand. In acoustics, a resistive screen can be made of a thin porous material and the simplest realization is a very fine mesh cloth, referred to in the following as wire mesh. Through such a screen, the acoustic velocity is continuous and the pressure $p$, described elsewhere by the Helmholtz equation, $\nabla^2 p + k^2 p = 0$, makes a jump at the screen,

*maazfarooqui@gmail.com
†yves.auregan@univ-lemans.fr
‡vincent.pagneux@univ-lemans.fr

 

which is given by

$$[\partial_n p]_s = 0 \quad \text{and} \quad [p]_s = -(Z/ik)\partial_n p, \tag{1}$$

where $\partial_n$ denotes the normal derivative, $k = \omega/c_0$ is the wave number, $\omega$ is the frequency, $c_0$ is the speed of sound, and $Z$ is the screen impedance normalized by $\rho_0 c_0$, where $\rho_0$ is the density of the medium. With the $\exp(-i\omega t)$ convention that is chosen here, there is absorption if $\Re(Z) > 0$. As long as viscous effects dominate inertial effects, this screen is purely resistive, $|\Im(Z)| \ll \Re(Z)$, and the resistance is proportional to the viscosity and depends on the wire diameter, the type of weave, and the size of the apertures. Consequently, the purely resistive wire mesh considered in the following is modeled by a positive real $Z$ independent of the frequency.

Due to its high flexibility and to avoid vibration, it is advantageous to bond the wire mesh to a more rigid perforated plate (see Fig. 1; in the following, the assembly of these two thin parts will simply be called wire mesh). The resistance of the assembly is then given by the product of the intrinsic resistance of the wire mesh and the percentage of open area (POA) of the perforated plate (see more details in Appendix A).

In the particular case of a plane wave at normal incidence to the screen, the problem becomes unidimensional and the reflection and transmission coefficients are written as

$$R = Z/(2+Z) \quad \text{and} \quad T = 2/(2+Z), \tag{2}$$

while the absorption coefficient for an incident wave on one side is

$$\alpha = 1 - |R|^2 - |T|^2 = \frac{1}{2}\left(1 - \left|\frac{Z-2}{Z+2}\right|^2\right). \tag{3}$$

The resistance $Z = 2$ maximizes the absorption coefficient of the screen, $\alpha = 1/2$, when the incident wave is only on one side of the screen [10,18]. In this case, the reflection and transmission coefficients are also equal to

$$R = T = 1/2. \tag{4}$$

Figure 2(b) displays the measured reflection ($R$) and transmission ($T$) coefficients of an assembly of wire mesh of resistance 1.02 with a perforated plate with a POA of 50%, leading to an impedance very close to $Z = 2$. These measured coefficients are nearly equal to 1/2 in a hyperwide frequency band extending from zero frequency to the maximum measurement frequency given by the cutoff frequency of the measuring tube.

The two singular values (SVs) of the scattering matrix,

$$S = \begin{pmatrix} R & T \\ T & R \end{pmatrix}, \tag{5}$$

correspond to the maximum and minimum outgoing wave fluxes for any incoming waves with unit flux. They are given by

$$\sigma_S = 1 \quad \text{and} \quad \sigma_A = \left|\frac{Z-2}{Z+2}\right|, \tag{6}$$

which correspond, respectively, to the symmetric [Fig. 2(c)] and antisymmetric [Fig. 2(d)] cases [19]. When $Z = 2$, these SVs are theoretically as well as experimentally equal to 1 and 0 [see Fig. 2(b)]. In the symmetric case, there is no dissipation and everything works as if the screen was not present. In the antisymmetric case, the waves are completely absorbed and the screen becomes a CPA [5,20]. In

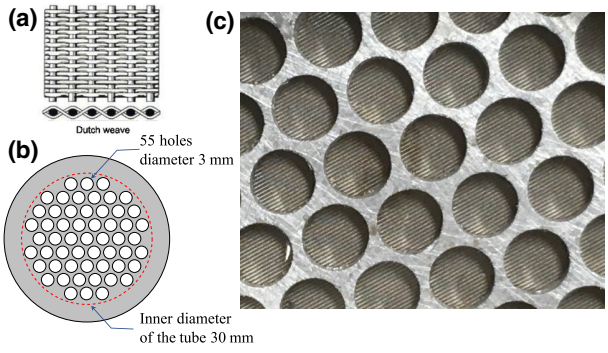


FIG. 1. (a) The wire mesh is made of stainless-steel fabric with a Dutch weave. (b),(c) To prevent the wire mesh from vibrating, the wire mesh is glued to a perforated steel support plate.

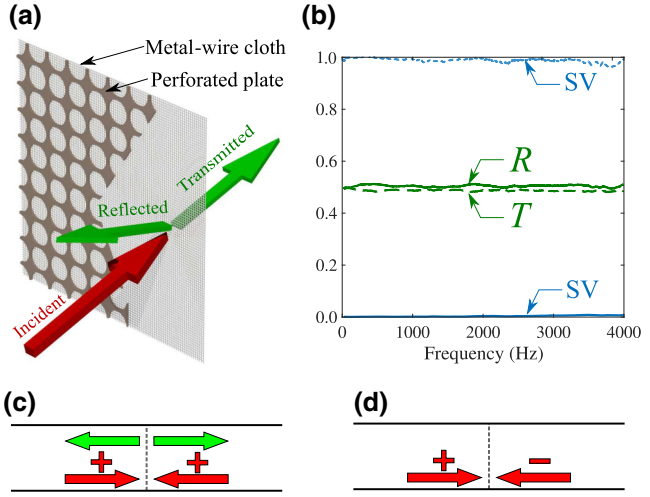


FIG. 2. A generic wire-mesh absorber. (a) A schematic of the absorber illuminated by a unidirectional acoustic wave. (b) The measured absolute values of the reflection, $|R|$, and transmission, $|T|$, coefficients. The SVs are the measured singular values of the scattering matrix. (c),(d) Symmetric (c) and antisymmetric (d) cases displaying zero and perfect absorption, respectively.

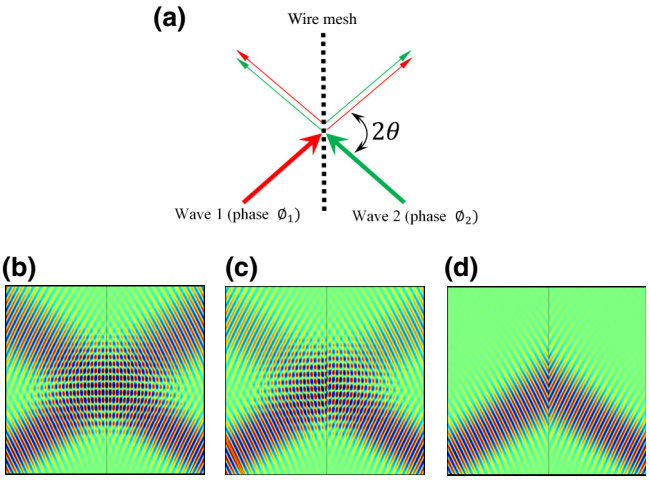


FIG. 3. The numerical simulation of an incident Gaussian beam on wire mesh, $Z = 2/\cos(\theta)$. (a) A schematic drawing of the wire mesh with incident Gaussian beams at oblique angle $\theta = \pi/6$. (b) The symmetric case, $\phi_1 - \phi_2 = 0$. (c) The intermediate case, $\phi_1 - \phi_2 = \pi/2$. (d) The antisymmetric case, $\phi_1 - \phi_2 = \pi$.

particular, it can be noted that the measured singular value $\sigma_A$ that corresponds to the CPA never exceeds 0.008 for all measured frequencies.

This CPA effect is further illustrated in Fig. 3, where two Gaussian beams of the same amplitude are incident on the screen with the same angle $\theta$ and at the same point. In this case, $\sigma_S = 1$ and $\sigma_A = |(\cos(\theta)Z - 2)/(\cos(\theta)Z + 2)|$. Thus the optimal impedance varies according to the inclination of the wave, with $Z = 2/\cos(\theta)$. It can be seen that when the two waves are in phase [Fig. 3(b)] the waves propagate, far from the screen, as if the screen was not there. On the contrary, when the two incident waves are of opposite phase [Fig. 3(d)], they are completely absorbed (CPA). For an intermediate phase, the waves are partially absorbed [Fig. 3(c)].

In view of the previous results, it appears that the use of a wire-mesh resistive screen in acoustics leads to CPA with a huge subwavelength ratio. In our experiment, the total thickness of the wire mesh is 1.2 mm, while the lowest measured frequency is 50 Hz (see Fig. 2): this leads to a subwavelength ratio of 6800 as well as a hyperwide frequency band. We insist that the prefix "hyper" refers here to the fact that the CPA operates from the zero-frequency limit (here measured down to 50 Hz due to loudspeaker limitations) to the cutoff frequency of the duct (here around 6 kHz).

## III. SYMMETRIZATION IN THE TIME DOMAIN

An interesting aspect is that such a large bandwidth opens up the possibility of extending the CPA effect into the time domain. For a scattering problem, it would be obvious that short wave packets incident from both sides and with good phase adjustment would lead to total absorption (by a simple Fourier-transform argument of the previous results). We now choose to go one step further by using the symmetry of closed cavities to provide the phase-coherence ingredient in CPA. Indeed, it appears that a mirror-symmetric cavity naturally allows us to decompose the wave into components with different parities (i.e., symmetric and antisymmetric). Thus, with parity and phase coherence coming together, the CPA effect is accomplished by locating the wire mesh at the symmetry axis. To explore this aspect in an actual experiment, we consider a closed duct of length $2L$ ($L = 405$ mm) in which the CPA wire mesh (with $Z = 2$) is placed at the midposition (the symmetry axis). At the left extremity of the duct, we send a pulse through a small orifice [21] and two microphones $M_1$ and $M_2$ are located at the two extremities [see Fig. 4(a)]. The incident pulse signal is measured at $M_1$ by windowing the multiple echoes [Fig. 4(b)]. First, as a reference, when the wire mesh is not present, the pressure signals are displayed in Fig. 4(c), where the incident pulse is reproduced every $4\tau$ (where $\tau = L/c_0 = 1.18$ ms is half the time of flight between the two microphones), since the wave is reflected at both extremities of the duct [22]. Then, in the presence of the wire mesh, the situation is clearly different, with equal signals at both ends from early time $2\tau$ [Fig. 4(d)]. The reason for this symmetrization of the pressure in the duct is simple: when the pulse reaches the screen (at time $\tau$), it is half transmitted and half reflected

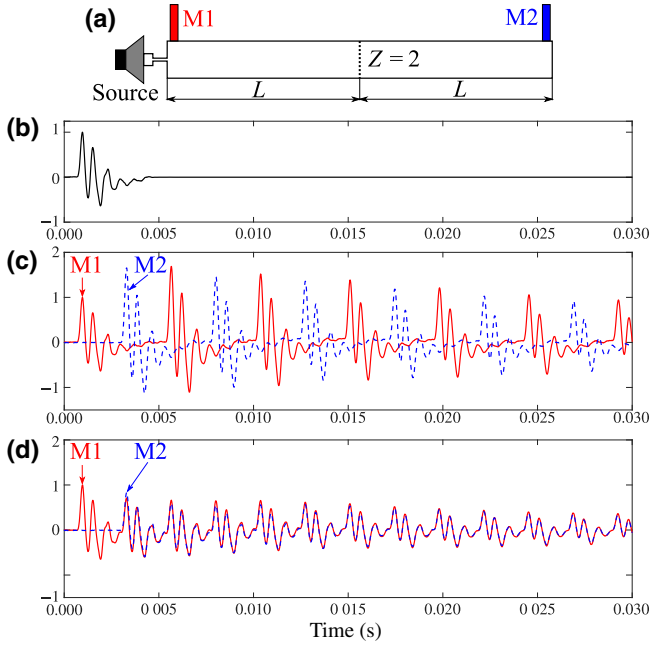


FIG. 4. The measured temporal signals. (a) A sketch of the experimental setup. (b) The input signal from the source. (c) The measured responses at microphones M1 (solid red) and M2 (dashed blue) for an empty tube. (d) The measured responses at M1 and M2 for a tube with $Z = 2$ wire mesh.

and, from that instant, the sound field becomes completely symmetric with respect to the middle of the duct, reaching the symmetric microphones at $2\tau$. It can be noted that the equal amplitudes of the two pulses on each side of the screen correspond to half the amplitude of the incident wave.

## IV. SYMMETRIZATION IN THE FREQUENCY DOMAIN

The symmetrization of the acoustic field by introducing a CPA wire mesh at the symmetry axis of a cavity can also be observed in the frequency-response spectrum. In the same experimental setup as described above, in order to detect the resonance frequencies of the closed duct, we now measure the transfer function, defined as the ratio of the pressure at microphone M2 to the voltage applied to the source (approximately proportional to the flow rate of the source; see Fig. 5). Without wire mesh (red line), the peaks correspond to the modes of a closed tube of length $2L$ and are given by $f_n = nc_0/4L$, where $c_0/4L = 211.5$ Hz and $n = 1, 2, \ldots$ When the wire mesh is inserted at the midposition of the tube (dashed blue line), half of the modal resonances are suppressed. The cutoff resonances correspond to antisymmetric modes, while the resonances associated with symmetric modes remain unchanged. This effect of suppression of the antisymmetric modes and thus of symmetrization of the resonances is described in Appendix A by a simple one-dimensional model.

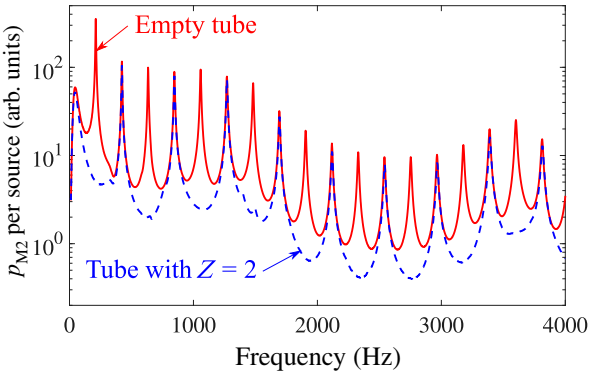


FIG. 5. Experimental results for the transfer function of the pressure $p_{M2}$ referred to the source in the same geometry as in Fig. 4(a) for an empty tube (solid red) and for a tube with $Z = 2$ wire mesh (dashed blue).

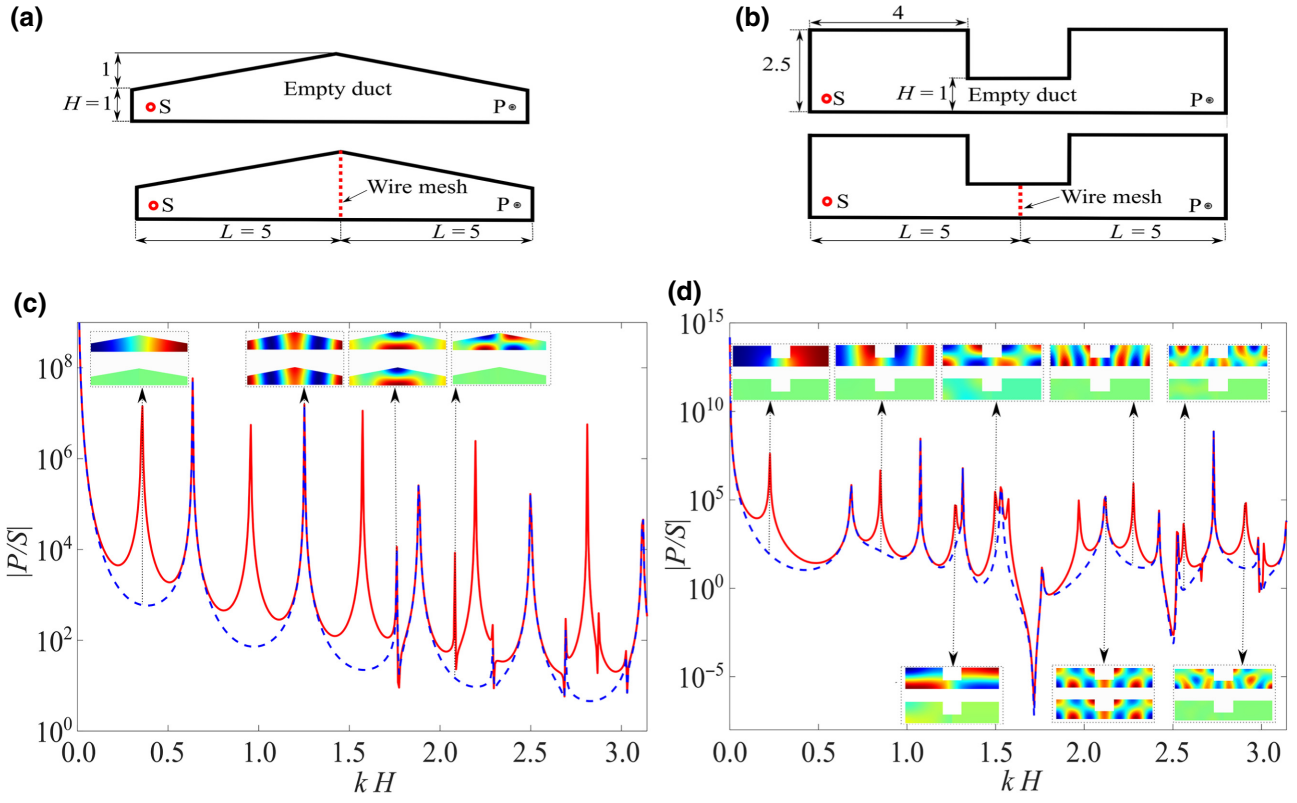


FIG. 6. Transfer-function $|P/S|$ calculations for ducts of variable cross section with and without $Z = 2$ wire mesh, where $S$ is a monopole-source strength at point S and $P$ is the pressure at point P. (a) The empty bitriangular geometry (top) and that with $Z = 2$ wire mesh (bottom). (b) The empty cavity-loaded geometry (top) and that with $Z = 2$ wire mesh (bottom). (c) The variation of $|P/S|$ with respect to $k$ for bitriangular ducts. (d) The variation of $|P/S|$ with respect to $kH$ for cavity-loaded ducts.

Rather surprisingly, this antisymmetric mode suppression by a resistive screen is robust to geometric changes and is maintained even when the symmetric geometry has a variable cross section. To illustrate this phenomenon, two different symmetric geometries are considered in Fig. 6. The first is a bitriangular duct [Fig. 6(a)], while the second is a duct connected to symmetric lateral cavities [Fig. 6(b)]. For a given source at point S, the frequency-response spectrum at point P is numerically computed using COMSOL Multiphysics and the results are displayed in Figs. 6(c) and 6(d), with and without a resistive screen of impedance $Z = 2$ located in the symmetry plane. It appears that the resonances associated with antisymmetric modes are suppressed for both geometries as in the constant-section case. Thus the antisymmetric suppression occurs even when the waves are not plane and normal to the wire mesh. We can see such behavior in Fig. 6(a), for the mode at $kH = 2.1$, which exhibits that wire mesh is effective even on higher-order modes. However, the suppression effect is possibly diminished for modes with a high angle of inclination on the wire mesh, as in Fig. 6(d) at $kH = 1.5$.

## V. CONCLUSIONS

This work demonstrates, experimentally and theoretically, the control of antisymmetric acoustic waves in ducts using an ultrathin resistive screen. It is based on the concept of coherent perfect absorption and since the ultrathin sheets are of a purely resistive nature, their effects are not linked to a resonance phenomenon. Consequently, the symmetrization of the acoustic waves is extremely broadband, starting from zero frequency, and can even be exhibited in the time domain with short pulses. In addition, it is shown that this symmetrization effect is robust to variations of the duct cross section. This work opens up the possibility of creating ultrathin noise controllers and attenuators that are simultaneously extremely broadband and ultrasubwavelength.

## ACKNOWLEDGMENTS

This work was supported by the International Agence Nationale de la Recherche (ANR) project FlowMatAc, "Experimental and numerical studies of an innovative acoustical material technology for industrial and urban flow noise mitigation," cooperative project between France and Hong Kong (Grant No. ANR-15-CE22-0016-01). We thank Svetlana Kuznetsova, Christian Morfonios, and Malte Rontgen for their careful reading of the manuscript.

## APPENDIX A: PRACTICAL REALIZATION OF THE RESISTIVE SHEET

The wire mesh used in this study is a stainless-steel fabric with a Dutch weave [see Fig. 1(a)]. The wire diameters are 0.050 mm for the warp and 0.036 mm for the weft.

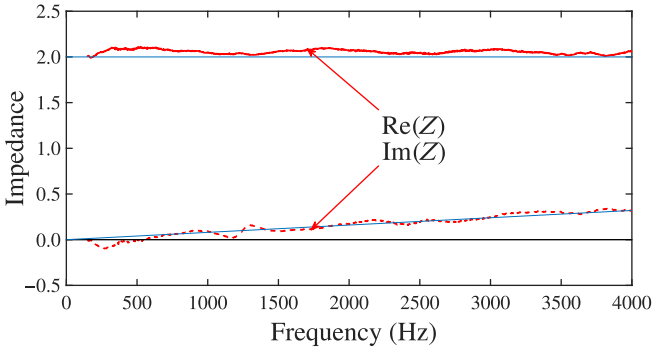


FIG. 7. The measured impedance value of the wire mesh glued on its support plate.

When it is used alone, this wire mesh has a static resistance of $Z_{\mathrm{WM}} = \Delta p/\rho_0 c_0 U = 1.13$, where $\Delta p$ is the pressure drop across the wire mesh when it is exposed to a flow of velocity $U$. To prevent the wire mesh from vibrating, it is glued to a 0.8-mm-thick steel support plate [see Fig. 1(c)]. This disk is perforated with 55 holes of 3 mm diameter [see Fig. 1(b)]. Compared to a tube with an internal diameter of 30 mm, the percentage of open area (POA) is therefore 0.55. The expected resistance is $Z = Z_{\mathrm{WM}}/\mathrm{POA} = 2.05$. The measured impedance is given in Fig. 7, where it can be seen that the resistance is close to the expected value and the imaginary part is small, especially at low frequencies.

## APPENDIX B: ONE-DIMENSIONAL MODEL OF THE CAVITY WITH A RESISTIVE SHEET

To compute the modes in a duct of length $2L$ with thin wire mesh at the center (see Fig. 8), the acoustic field can be written as $p_1 = A_1 \cos(kx)$ for $0 < x < L$ and $p_2 = A_2 \cos(k(2L - x))$ for $L < x < 2L$. At the wire-mesh position, the continuity of velocity and the impedance relation that can be written as

$$[p']_L = 0 \quad \text{and} \quad [p]_L = (-Z/ik)p', \tag{B1}$$

which leads to

$$(A_1 + A_2)\sin(kL) = 0, \tag{B2}$$

$$(A_1 - A_2)\cos(kL) = iZA_1 \sin(kL), \tag{B3}$$

which eventually leads to the dispersion relation

$$\mathcal{D} = \sin(kL)(2\cos(kL) - iZ\sin(kL)) = 0. \tag{B4}$$

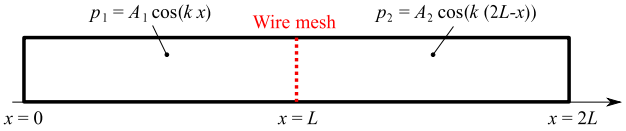


FIG. 8. One-dimensional analysis of the acoustic field in a duct with thin wire mesh.

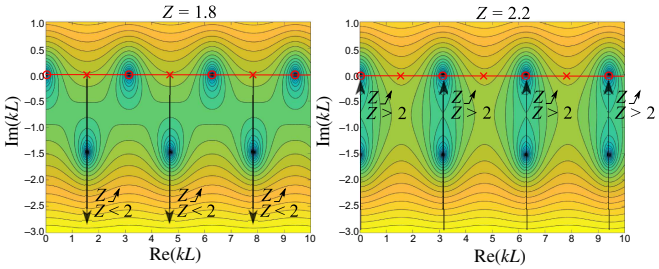


FIG. 9. The color map of $|\mathcal{D}|$ for two values of the resistance $Z$. The blue values correspond to $|\mathcal{D}| = 0$. Symmetric modes marked with red circles do not move. The antisymmetric modes (indicated by a red "×" at $Z = 0$) acquire a negative imaginary part when $Z$ moves away from 0. The imaginary part becomes larger and larger until the modes disappear at infinity for $Z = 2$. For a resistance higher than 2, these modes return from infinity to the symmetric modes (red circles).

When $Z = 0$, two sets of solutions exist: one with $\sin(kL) = 0$ ($A_1 = A_2$) and the other with $\cos(kL) = 0$ ($A_1 = -A_2$). They correspond, respectively, to the symmetric and antisymmetric modes of the empty tube of length $2L$.

When $Z$ is different from 0, the symmetric modes ($\sin(kL) = 0$ and $A_1 = A_2$) retain real eigenfrequencies $k$; in fact, they do not feel the presence of the wire mesh, because $p' = 0$ at $x = L$ [see Eq. (B1)]. On the other hand, the eigenfrequencies of the antisymmetric modes are no longer real, as can be seen in Fig. 9. These modes progressively acquire a negative imaginary part, while their real parts remain equal to $n\pi/2$ ($n = 1, 2, 3, \ldots$). For $Z = 2$, these modes disappear with an imaginary part that tends to infinity. For a resistance higher than 2, they reappear from infinity and return to the symmetric modes with a real part equal to $m\pi$ ($m = 0, 1, 2, \ldots$). Why is $Z = 2$ so special for the antisymmetric modes? This can be seen if we use the symmetry of the system, which allows us to decompose the eigenproblem into two subproblems; one for the symmetric modes and the other for the antisymmetric modes. For the antisymmetric problem, we arrive at the wave equation with boundary conditions: $p = 0$ at $x = 0$ and $ikp = (Z/2)p$ at $x = L$. It is then clear that for $Z = 2$, these boundary conditions ($p = 0$, i.e., a hard wall, and $p = ikp$, i.e., the wave totally radiating to the right) correspond to the problem of a semi-infinite tube, which is known to have no resonance frequencies at all.

### 1. Calculations with a source

When a point source is placed inside a rigid duct at $x = x_0$ (see Fig. 10), the Helmholtz equation with a point source can be written in the form

$$p'' + k^2 p = \delta(x - x_0). \tag{B5}$$

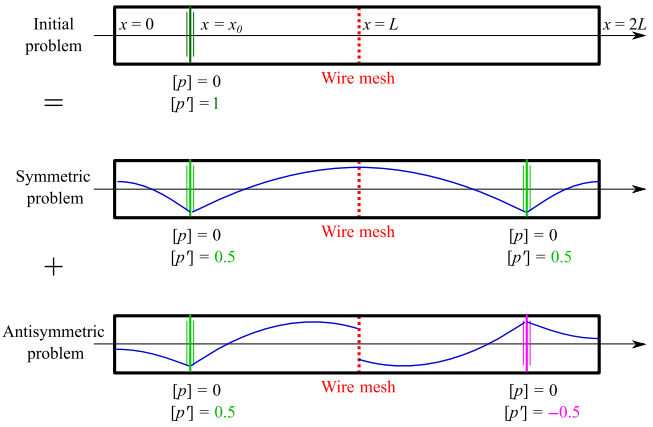


FIG. 10. The one-dimensional problem in a duct in the presence of wire mesh and with a source considered as the addition of a symmetric problem and an antisymmetric problem.

The presence of the source at $x = x_0$ gives two relations linking the pressure and its derivative on both sides of the source at $x = x_0$: $[p']_{x_0} = 1$ and $[p]_{x_0} = 0$. To simplify the solution of this problem, it can be considered as the sum of two problems, one symmetric and the other antisymmetric: $p(x) = p_s(x) + p_a(x)$ (see Fig. 10).

For the symmetric problem, the pressure derivative always vanishes on the wire mesh ($x = L$), which can therefore be considered as a rigid wall ($p_s'(L) = 0$). The symmetric solution can then be written as

$$\begin{aligned} p_s &= S_1 \cos(kx) \quad 0 < x < x_0, \\ p_s &= S_2 \cos(k(x - L)) \quad x_0 < x < L, \end{aligned}$$

where $S_1$ and $S_2$ are given by

$$\begin{aligned} 2k \sin(kL) S_1 &= -\cos(k(L - x_0)), \\ 2k \sin(kL) S_2 &= -\cos(kx_0). \end{aligned}$$

For the antisymmetric problem, the pressure and its derivative for $x < L$ are linked at the wire mesh by

$$p_a(L) = \frac{Z}{2ik} p_a'(L). \tag{B6}$$

Then, the antisymmetric pressure can be written as

$$\begin{aligned} p_a &= A_1 \cos(kx) \quad 0 < x < x_0, \\ p_a &= A_2(\sin(k(L - x)) + iZ/2 \cos(k(L - x)) \quad x_0 < x < L, \end{aligned}$$

where $A_1$ and $A_2$ are given by

$$\begin{aligned} k[2\cos(kL) - iZ\sin(kL)]A_1 \\ = iZ/2 \cos(k(L - x_0)) + \sin(k(L - x_0)), \\ k[2\cos(kL) - iZ\sin(kL)]A_2 = \cos(kx_0). \end{aligned}$$

A plot of these solutions is given in Fig. 11.

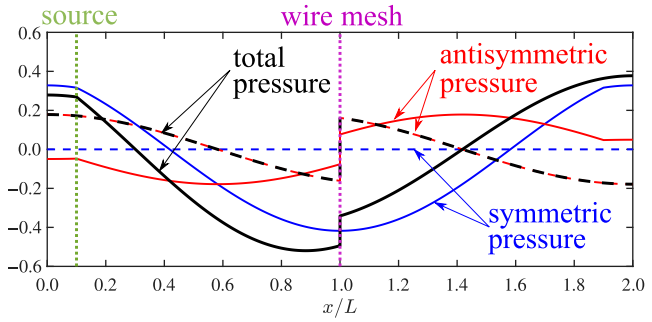


FIG. 11. The pressure in the tubes for $Z = 2$, $kL = 2.7$, and $x_0 = 0.1L$. The solid lines are the real part of the pressure, while the dashed lines are the imaginary part: blue, symmetric pressure $p_s$; red, antisymmetric pressure $p_a$; black, total pressure $p = p_s + p_a$.

In order to compare these one-dimensional results with the experimental results, the source is placed on one of the walls by setting $x_0 = 0$. The pressure is calculated at the point where there is a microphone, i.e., at $x = 2L$. The total pressure at the microphone is then equal to $p_t(2L) = p_s(0) - p_a(0)$. The symmetric and antisymmetric pressure are as follows:

$$p_s(0) = -\frac{\cos(kL)}{2k\sin(kL)},$$
$$p_a(0) = \frac{2\sin(kL) + iZ\cos(kL)}{2k(2\cos(kL) - iZ\sin(kL))}.$$

As can be seen in Fig. 12, the calculations compare qualitatively well with the experimental results: the presence of wire mesh of resistance $Z = 2$ makes the antisymmetric modes disappear. A more quantitative comparison is not possible here, because the acoustic flow rate of the source is not measured during the experiments. The one-dimensional calculations can therefore be used quite easily to predict the effect of a resistive sheet in a tube (see Fig. 13).

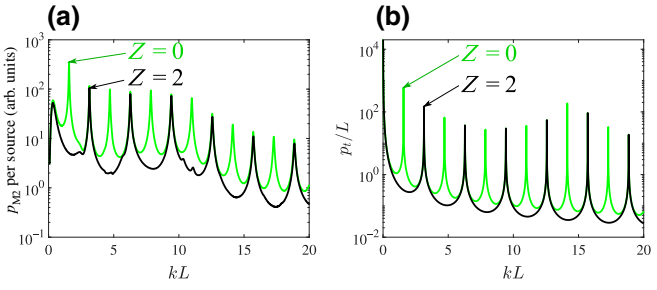


FIG. 12. A comparison of the ratio between the pressure at $x = 2L$ and the source at $x = 0$: (a) experimental results; (b) one-dimensional calculations. The green curves correspond to an empty tube ($Z = 0$) and the black curves to a tube with wire mesh with $Z = 2$. We see that half of the resonance peaks (corresponding to antisymmetric modes) are suppressed for $Z = 2$.

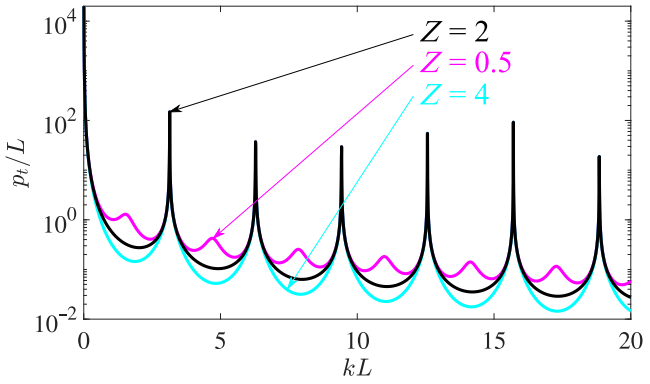


FIG. 13. The ratio between the pressure at $x = 2L$ and the source at $x = 0$ for three different values of the resistance: black, $Z = 2$; magenta, $Z = 0.5$; cyan, $Z = 4$.


[1] N. I. Landy, S. Sajuyigbe, J. J. Mock, D. R. Smith, and W. J. Padilla, Perfect Metamaterial Absorber, Phys. Rev. Lett. **100**, 207402 (2008).

[2] C. M. Watts, X. Liu, and W. J. Padilla, Metamaterial electromagnetic wave absorbers, Adv. Mater. **24**, OP98 (2012).

[3] J. Mei, G. Ma, M. Yang, Z. Yang, W. Wen, and P. Sheng, Dark acoustic metamaterials as super absorbers for low-frequency sound, Nat. Commun. **3**, 1 (2012).

[4] M. Yangand and P. Sheng, Sound absorption structures: From porous media to acoustic metamaterials, Annu. Rev. Mater. Res. **47**, 83 (2017).

[5] Y. Chong, L. Ge, H. Cao, and A. D. Stone, Coherent Perfect Absorbers: Time-Reversed Lasers, Phys. Rev. Lett. **105**, 053901 (2010).

[6] W. Wan, Y. Chong, L. Ge, H. Noh, A. D. Stone, and H. Cao, Time-reversed lasing and interferometric control of absorption, Science **331**, 889 (2011).

[7] D. G. Baranov, A. Krasnok, T. Shegai, A. Alù, and Y. Chong, Coherent perfect absorbers: Linear control of light with light, Nat. Rev. Mater. **2**, 1 (2017).

[8] A. Müllers, B. Santra, C. Baals, J. Jiang, J. Benary, R. Labouvie, D. A. Zezyulin, V. V. Konotop, and H. Ott, Coherent perfect absorption of nonlinear matter waves, Sci. Adv. **4**, eaat6539 (2018).

[9] P. Wei, C. Croënne, S. Tak Chu, and J. Li, Symmetrical and anti-symmetrical coherent perfect absorption for acoustic waves, Appl. Phys. Lett. **104**, 121902 (2014).

[10] C. Meng, X. Zhang, S. T. Tang, M. Yang, and Z. Yang, Acoustic coherent perfect absorbers as sensitive null detectors, Sci. Rep. **7**, 43574 (2017).

[11] S. Longhi, Backward lasing yields a perfect absorber, Physics **3**, 61 (2010).

[12] M. Yang, S. Chen, C. Fu, and P. Sheng, Optimal sound-absorbing structures, Mater. Horiz. **4**, 673 (2017).

[13] Y. Aurégan, Ultra-thin low frequency perfect sound absorber with high ratio of active area, Appl. Phys. Lett. **113**, 201904 (2018).

[14] G. Nimtzand and U. Panten, Broad band electromagnetic wave absorbers designed with nano-metal films, Ann. Phys. **19**, 53 (2010).
[15] S. Li, J. Luo, S. Anwar, S. Li, W. Lu, Z. H. Hang, Y. Lai, B. Hou, M. Shen, and C. Wang, Broadband perfect absorption of ultrathin conductive films with coherent illumination: Superabsorption of microwave radiation, Phys. Rev. B **91**, 220301 (2015).
[16] U. Ingard, *Noise Reduction Analysis* (Jones & Bartlett, Sudbury, 2009).
[17] A. Coutant, Y. Aurégan, and V. Pagneux, Anomalous transmission through periodic resistive sheets, J. Acoust. Soc. Am. **147**, 3124 (2020).
[18] E. Plum, K. F. MacDonald, X. Fang, D. Faccio, and N. I. Zheludev, Controlling the optical response of 2D matter in standing waves, ACS Photonics **4**, 3000 (2017).
[19] A. Merkel, G. Theocharis, O. Richoux, V. Romero-García, and V. Pagneux, Control of acoustic absorption in one-dimensional scattering by resonant scatterers, Appl. Phys. Lett. **107**, 244102 (2015).
[20] V. Romero-García, G. Theocharis, O. Richoux, A. Merkel, V. Tournat, and V. Pagneux, Perfect and broadband acoustic absorption by critically coupled sub-wavelength resonators, Sci. Rep. **6**, 19519 (2016).
[21] The small size of the orifice, the diameter of which is 1 mm, compared to the diameter of the duct (30 mm), makes it possible to consider that it has little influence on the acoustic response of the duct cavity.
[22] It can be noted that since the microphones are very close to the walls, they measure at the same time both the incident wave and the reflected pulses and the signal is doubled compared to the incident pulse.